Mapping hurricane damage: A comparative analysis of satellite monitoring methods

Matthew J. McCarthy[a,*], Brita Jessen[b], Michael J. Barry[c], Marissa Figueroa[b], Jessica McIntosh[b,d], Tylar Murray[a], Jill Schmid[b,d], Frank E. Muller-Karger[a]

[a] Institute for Marine Remote Sensing, College of Marine Science, University of South Florida, 140 7th Ave. South, Saint Petersburg, FL 33701, USA
[b] Rookery Bay National Estuarine Research Reserve, Florida Department of Environmental Protection, 300 Tower Rd, Naples, FL 34113, USA
[c] Tatenda, Inc., 5800 SW 188th Ave., Southwest Ranches, FL 33332, USA
[d] Center for Coastal Oceans Research, Institute of Water and Environment, Florida International University, Miami, FL 33199, USA

ABSTRACT

Wetlands are the second-most valuable natural resource on Earth but have declined by approximately 70 % since 1900. Restoration and conservation efforts have succeeded in some areas through establishment of refuges where anthropogenic impacts are minimized. However, these areas are still prone to wetland damage caused by natural disasters. Severe storms such as Hurricane Irma, which made landfall as a Category 3 hurricane in southwest Florida (USA) on September 11, 2017, can cause the destruction of mangroves and other wetland habitat. Multispectral images from commercial satellites provide a means to assess the extent of the damage to different wetland habitat types with high spatial resolution (2 m pixels or finer) over large areas. Using such images presents a number of challenges, including deriving consistent and accurate classification of wetland and non-wetland vegetation. Machine learning methods have demonstrated high-accuracy mapping capabilities on small spatial scales, but require a large amount of robust training data. Meanwhile, ambitious efforts to map larger areas at finer resolutions may use hundreds of thousands of images, and therefore encounter Big-Data processing challenges. Large-scale efforts face the dilemma of adopting traditional mapping methods that may lend themselves to Big Data analytics but may result in accuracies that are inferior to new methods, or move to machine learning methods, which require robust training data. Given these considerations, we describe a version of the traditional Decision Tree (DT) approach and compare two common machine learning methods to derive land cover classes using a WorldView-2 image collected on November 12, 2018 to include one growing season after Hurricane Irma affected this area. Specifically, we compared the Support Vector Machine [SVM] and Neural Network [NN] methods, trained and validated with separate ground-truth datasets collected during a robust field campaign. Overall accuracies were only marginally different (85 % NN vs 83 % each DT and SVM), but healthy mangroves were more accurately identified with the DT (91 % vs 88 % NN and 86 % SVM), and degraded mangroves were more accurately identified with NN (62 % vs 57 % NN and 38 % DT). These results, combined with their respective training requirements, have implications for the direction with which large-scale high-resolution mapping of coastal habitats proceeds.

1. Introduction

Global coastal and freshwater wetlands have been lost to anthropogenic development by up to 71 % during the 20th century, and are expected to continue to decline at a rate of 1–3 % annually (Davidson, 2014; McLeod et al., 2011). Coastal wetlands are estimated to generate over $200,000 USD per hectare per year to local economies, and are areas of beneficial nutrient filtering, carbon sequestration, shoreline stabilization, flood prevention, and habitat for numerous species of fish,

birds, and invertebrates (de Groot et al., 2012; Barbier, 2015). Further, recent research suggests that better understanding and monitoring of wetland extent may fill vital knowledge gaps in understanding global greenhouse gas emissions (Nisbet et al., 2019; Turner et al., 2016). Filling these gaps and enhancing management capabilities to mitigate wetland decline requires accurate and updated maps to quantify wetland area and habitat composition (Klemas, 2013; Kuenzer et al., 2011).

A changing global climate (e.g. sea-level rise, altered drought and precipitation patterns, extreme storm events) and modification of
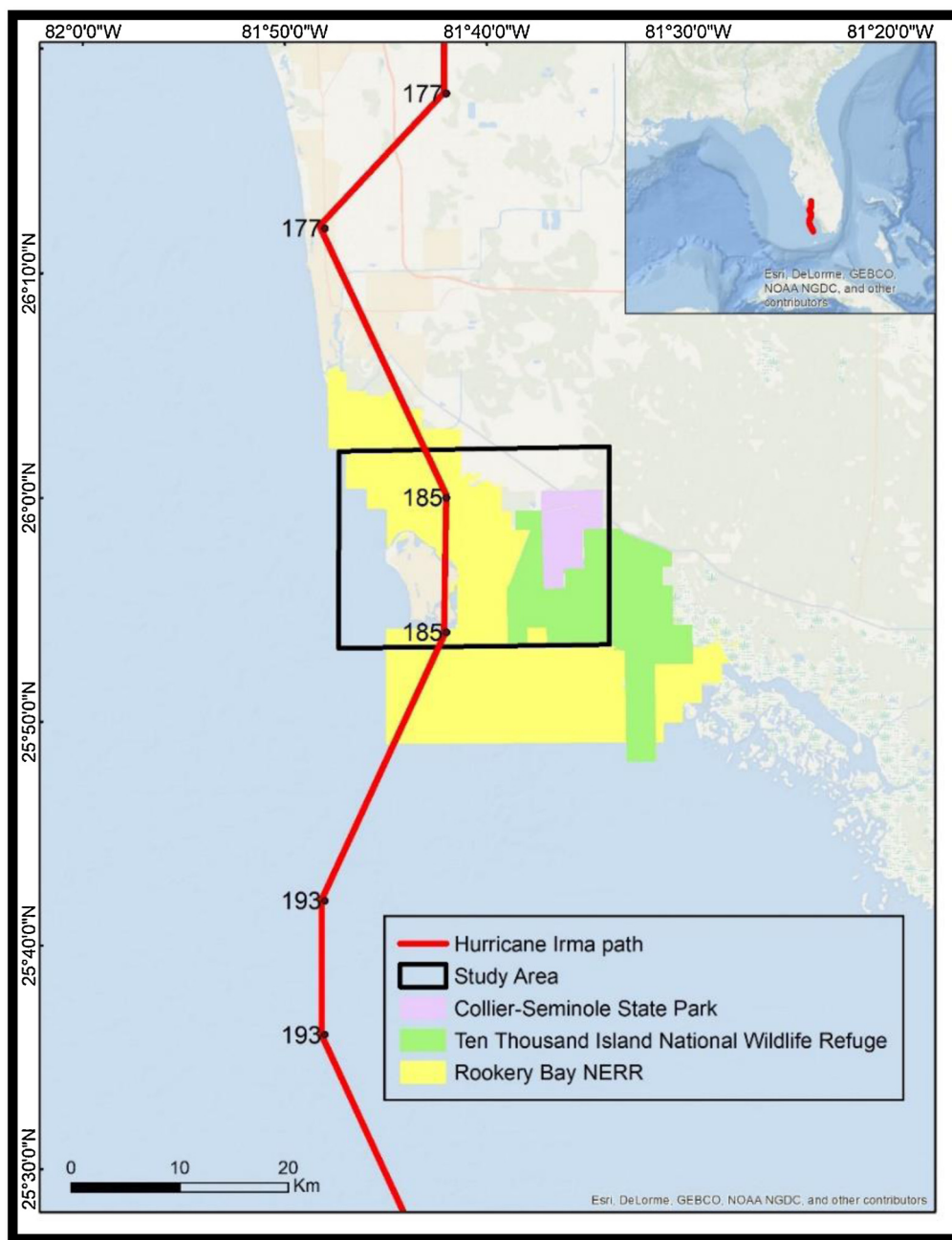

Fig. 1. Southwest Florida, USA, showing the path of Hurricane Irma (red line), and wind speeds (Km h^{-1}). Local management jurisdiction boundaries are shown in different colors. Study area is shown as a black box. (For interpretation of the references to color in this figure legend, the reader is referred to the web version of this article.)

coastal ecosystems by humans (e.g. coastal development, wetland drainage, hydrologic alterations) compound the stress to mangrove ecosystems. Swift and concerted action by local resource managers requires regular and up-to-date information on the location and extent of mangrove cover. This requires repeat monitoring of coastal habitats at very high spatial resolutions to facilitate local detection of change before it expands beyond the capacity of existing methods for conservation and restoration.

Technological advances have enhanced the spatial resolution of commercially-available satellite images by several orders of magnitude (e.g. 4 m^2 per pixel and better for WorldView-2 vs. ~900 m^2 per pixel for Landsat Thematic Mapper data). This has led to enhanced mapping precision and accuracy (Klemas, 2013; Kuenzer et al., 2011; Hestir et al., 2015; Turpie, 2013). Digital processing methods now allow

expanded and repeated resource mapping to regional scales at the relatively coarse Landsat resolution (Giri et al., 2011; Friedl et al., 2002). Improving such maps with higher spatial resolution increases the data processing requirements (i.e. data transfer time, storage capacity, and computation time) by up to several orders of magnitude, thereby necessitating the development of techniques to leverage the computational efficiency of supercomputers without compromising the high accuracies that are required of natural-resource maps used for management purposes. However, it appears as though two divergent approaches to coastal-habitat mapping are developing concomitantly: Large-scale (i.e. large-area), coarse-resolution mapping using traditional methods; and small-scale, high-resolution mapping with advanced machine-learning methods (Whyte et al., 2018; Liu et al., 2018; Hird et al., 2017). Effective coastal management will require a merging
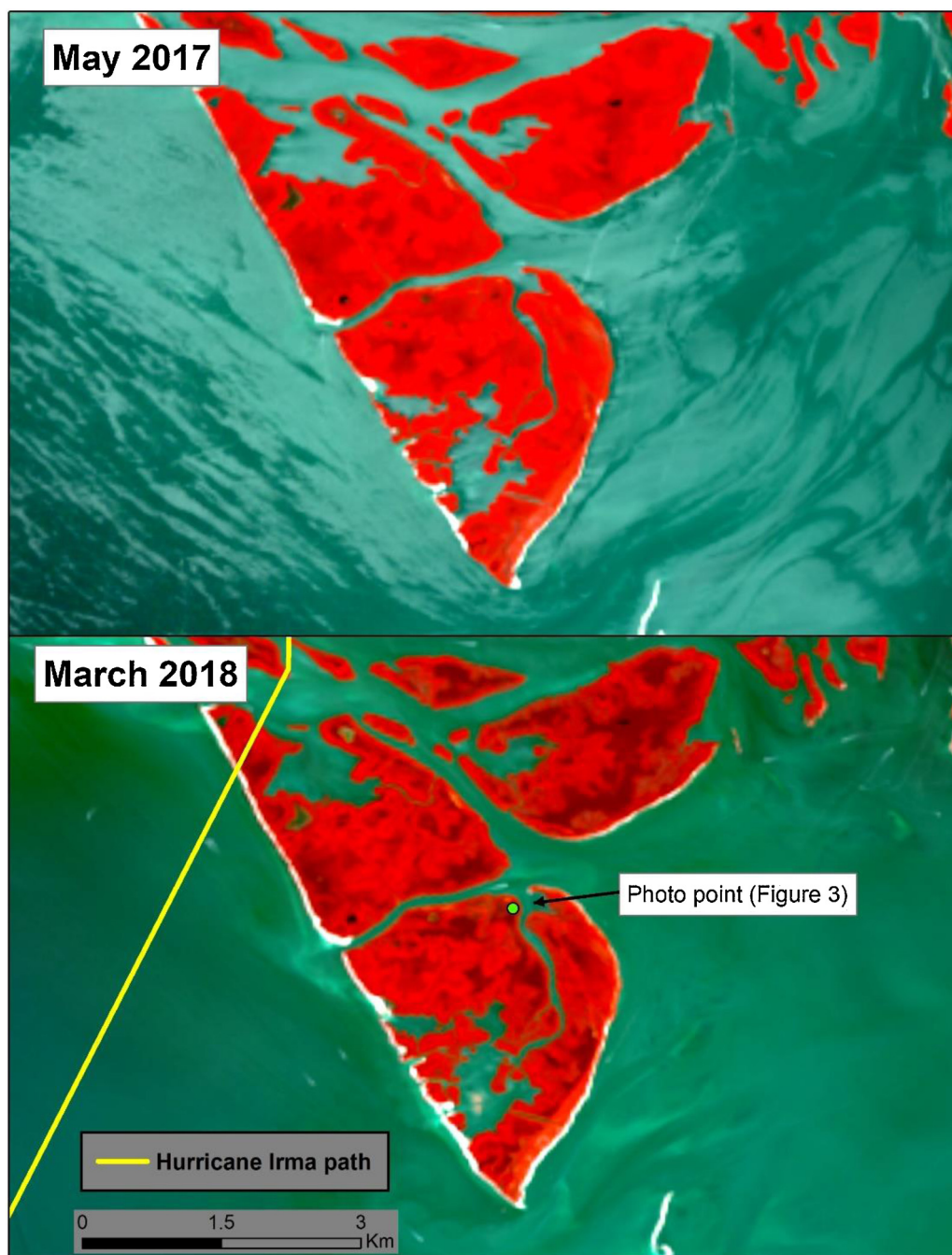
Fig. 2. False-color (near-infrared, green, blue band combinaton) Landsat satellite images (source: USGS) from before (**Top**) and after (**Bottom**) Hurricane Irma (yellow line) passed directly through the study area in September 2017. Dark patches in the March 2018 image indicate locations of severe mangrove forest defoliation (see Fig. 3). (For interpretation of the references to color in this figure legend, the reader is referred to the web version of this article.)

of these approaches that exploits the high resolution data by pairing it with accurate, automated mapping techniques that facilitate large-scale and repeat-monitoring application.

Among the most constraining elements of mapping of different land cover classes is the application of training data to develop accurate mangroves and non-mangrove vegetation classes, especially when these habitats are spectrally similar. Machine learning methods require robust ground-validation datasets (Scott et al., 2017; Shao and Lunetta, 2012). Training data are collected either by field campaigns (e.g. ground-truth GPS points), or by labeling of target map classes on preexisting multispectral imagery by a trained analyst (e.g. points or polygons manually drawn on target satellite images). The function of these data is to associate target habitat classes with the spectral

reflectance patterns of the associated satellite image pixels. Both field campaigns and manual digitization are time-consuming, and may be prohibitively expensive for large-scale mapping of a diverse set of habitats. A recent project that successfully mapped 65,000 km^2 stated that it required 10 years of field surveys to complete (Purkis et al., 2019).

Repeat mapping for the purpose of monitoring rapidly changing ecosystems requires at least some repeat ground-truthing. For example, if a hurricane defoliates a previously mapped healthy mangrove forest, the spectral signature of the forest will change, thus requiring new ground-truth data to incorporate this unique spectral signature into the mapping algorithm. Decision Tree classifiers built to use spectral libraries and historical data help ameliorate the effort by exploiting existing spectral data, algorithms and indices from the literature. This

Fig. 3. Photograph of defoliated black mangrove forest (see Fig. 2 for site location) from January 2019 site visit.

approach is routinely used for global-scale mapping of coarse imagery (Friedl et al., 2002).

Here we describe results of three different mangrove mapping methods to evaluate the impacts of Hurricane Irma, a Category 3 storm that affected southwest Florida in September of 2017. The approach was tested on a very high resolution WorldView-2 satellite image. The goals of this case study were (1) to compare the accuracies of these methods in distinguishing between healthy and degraded mangrove and non-mangrove vegetation, (2) to describe capabilities and pre-requisites of each method, and (3) to discuss these elements in the context of coastal habitat resource mapping on regional to global scales.

The study area intersects three management areas (Rookery Bay National Estuarine Research Reserve [NERR], Ten Thousand Islands National Wildlife Refuge, and Collier-Seminole State Park; Fig. 1).

Rookery Bay NERR is named for the mangrove rookery islands that dominate the landscape, along with marshlands, and upland habitat. The area was chosen because it is actively managed and the groups in charge of this process require spatial information on the extent and status of the wetlands. Further, Hurricane Irma made landfall within the study area after passing across the Caribbean and Florida Keys where it caused substantial damage to mangrove forests (Radabaugh et al., 2019; Walcker et al., 2019).

2. Materials and methods

Landsat satellite images were downloaded and evaluated for a preliminary assessment of the location and extent of the hurricane wind and flood damage to the mangrove forests of Rookery Bay NERR
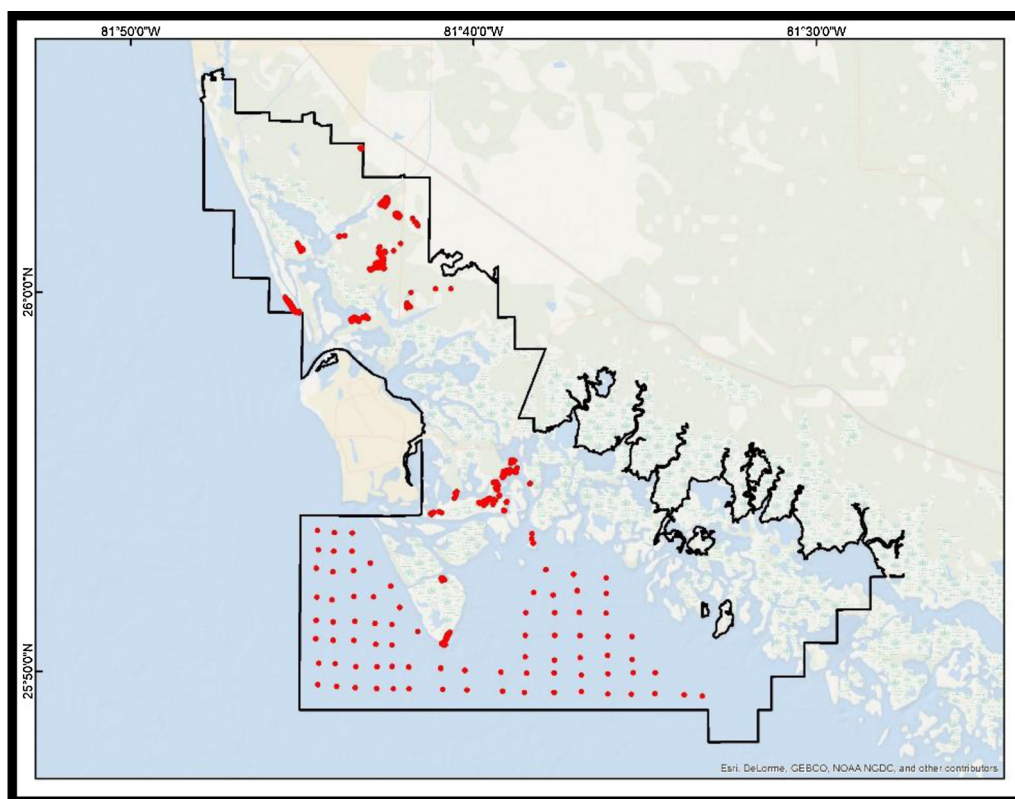
Fig. 4. Map of ground reference points acquired for training and accuracy assessment.

(Figs. 2 and 3).

We obtained one WorldView-2 NITF image (collected November 12, 2018; source: DigitalGlobe™; see (Globe, 2010) for a description of the data and (McCarthy and Halls, 2014) for a thorough evaluation of the uses of the eight multispectral bands for coastal habitat mapping). The image was preprocessed to apply a calibration provided by DigitalGlobe and converted to remote sensing reflectance (i.e., radiance measured at the spacecraft divided by downwelling solar irradiance). This conversion accounted for the Earth-Sun distance. A simple atmospheric correction was applied to remove Rayleigh atmospheric scattering (see McCarthy et al., 2018). The image was then classified using three methods: Decision Tree (DT); Neural Network (NN); and Support Vector Machine (SVM). The output was saved as a GeoTIFF for statistical analyses.

The DT classification approach is a binary, hierarchical, decision-based mapping method that assigns pixels a target land cover value by applying a series of "if" statements. The development of decisions represents the training aspect of this method, and required an analyst to study spectral patterns of target classes to identify patterns that could be leveraged through "if" statements to distinguish between classes.

The NN and SVM machine-learning methods require training data in the form of designated pixels (i.e. spectral data) labeled as one of the target classes. NN is a multivariate regression technique to evaluate non-normal, collinear, and nonlinear data (Lottering et al., 2019). Originally developed in the 1980s before being computationally tractable, NN has experienced a resurgence in recent years as artificial intelligence and deep learning approaches to feature extraction have advanced (Scott et al., 2017; Civco, 1993). Similarly, SVM was developed in the 1970's and experienced renewed interest in recent years as computational constraints have become less problematic. NN and SVM generally produce accurate results with limited training samples (Shao and Lunetta, 2012).

The November 2018 image acquisition coincided with a three-month (September-November 2018) field campaign that collected over 2700 GPS-based (3−5 m horizontal accuracy) ground-validation points throughout the Rookery Bay NERR study area. Quality control of ground-validation points required these criteria: located within the image tile; located at least 20 m from each other to avoid spatial autocorrelation; and clearly representative of healthy mangrove, degraded mangrove, upland (i.e. non-marsh grass and non-wetland forest), bare soil, or water. Mangroves were defined as belonging to the red (*Rhizophora mangle*), white (*Laguncularia racemosa*), or black (*Avicennia germinans*) species. Given these criteria, a total of 714 ground-truth points were selected (Fig. 4). These were randomly divided into two equal datasets representing training and validation data for the NN and SVM algorithms and mapped outputs from the DT, NN, and SVM. Accuracy assessment using the subset of 357 ground-truth points was conducted in ENVI™. Confusion matrices were generated for each map, including overall accuracy, User's Accuracies (i.e. commission error), and Producer's Accuracies (i.e. omission error).

3. Results

3.1. DT, NN, and SVM maps

Maps produced by each of the methods are shown in Fig. 5. Surface area (cover in km^2) of target classes is shown in Table 1, and area range from all three maps as a percent of total include soil (9–17 %), degraded mangrove (9–12 %), healthy mangrove (22–25 %), upland (9–16 %), and water (35–39 %). Each method correctly identified healthy mangrove as the dominant land cover throughout the study area. The greatest discrepancy in areal assignment was in the "soil" class. DT identified 56.6 km^2 (17 % of total area) as soil, whereas SVM and NN identified 35.9 km^2 (11 %) and 39.4 km^2 (12 %), respectively. This was likely due to the consistent misclassification of apparent cloud cover as soil. However, Fig. 5 highlights areas of mangrove degradation where classifiers differ in identifying mangrove vs soil, the latter of which in these areas would indicate dead or thoroughly defoliated mangrove
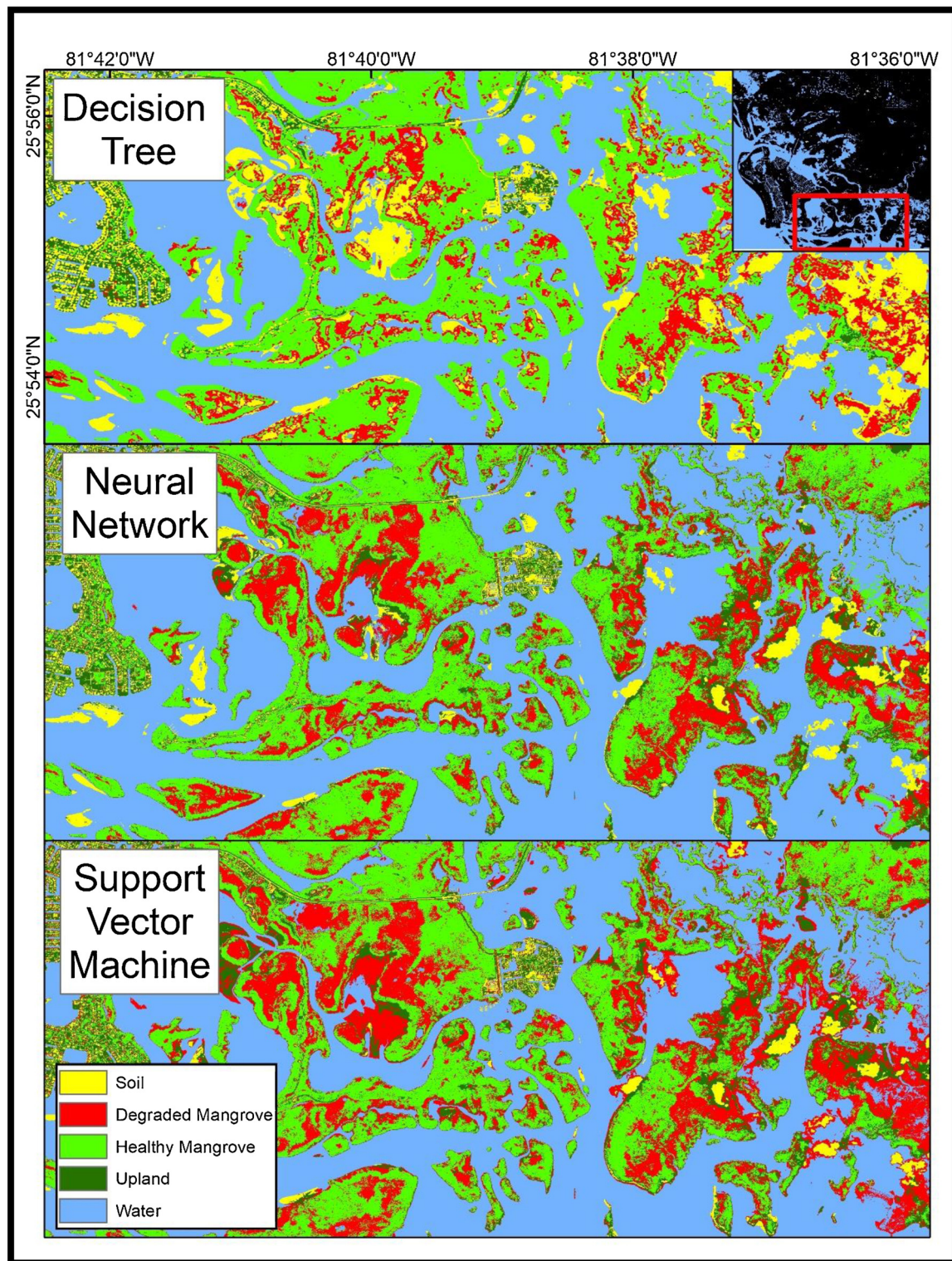
Fig. 5. Subset of study area where discrepancies between classifiers for soil, healthy mangrove, and degraded mangrove classes are most apparent.

such that the classifiers are identifying the soil beneath the defoliated canopies.

3.2. Accuracy assessments

Map accuracies were calculated with a confusion matrix for each classifier and are shown in Tables 2–4. Accuracies were determined by aligning GRPs with pixel data and comparing agreement. Producer's

accuracy reflects omission error or pixels that were incorrectly omitted from the correct class in the classified map. User's accuracy reflects commission error or pixels that were incorrectly included in each class in the classified map. Results include overall map accuracy, producer's accuracies, user's accuracies, and Kappa coefficient. The NN algorithm produced the most accurate overall map (85 %) versus 83 % for both DT and SVM. Individual class producer's accuracies, however, favored DT for healthy mangrove (91 % vs 88 % NN and 86 % SVM), NN for upland

Table 1
Area (km²) of target classes as identified by each method. "Unclassified" was not an output class for the trained SVM and NN methods. Total-area discrepancies are due to rounding.

Class	DT	SVM	NN
Soil	56.68	35.90	39.43
Degraded Mangrove	33.33	40.57	31.66
Healthy Mangrove	84.64	74.73	82.13
Upland	31.10	51.53	52.26
Water	116.92	131.38	128.63
Unclassified	11.27	NA	NA
Total	333.94	334.11	334.11

(75 % vs 69 % NN and 63 % DT), SVM for degraded vegetation (62 % vs 57 % NN and 38 % DT), DT for soil (97 % vs 92 % each NN and SVM), and all maps identified water to 100 % producer's accuracy.

4. Discussion

One of the objectives of this study was to place the comparative-analysis results in the context of future large-scale mapping and change-detection monitoring. Mapping wetlands for conservation and restoration purposes has long been a driver of finer-resolution, higher-accuracy remote sensing methods on local scales, but recent research into the role of wetlands in atmospheric greenhouse gas emissions and sequestration (i.e., blue carbon accounting), among other global-wetland research questions, necessitate expansion of these methods for large-scale monitoring. Measurements of atmospheric methane – second only to carbon dioxide in radiative forcing among anthropogenic greenhouse gases – indicate that concentrations have accelerated since 2007, and increased by more than 30 % over the past decade (Nisbet et al., 2019; Turner et al., 2016). Studies point to wetlands as a likely contributor to this acceleration (Dlugokencky et al., 2011; Bousquet et al., 2011; Bergamaschi et al., 2013; Pison et al., 2013), but note that there are substantial uncertainties with regard to wetland contribution due in part to poor monitoring of changes in global wetland area (Nisbet et al., 2019; Turner et al., 2016). That is, emissions from tropical wetlands increase exponentially with temperature, but vary as wetland area shrinks or grows with changes in precipitation (Nisbet et al., 2019; Gedney, 2004; McNorton et al., 2016g). Efforts to map global tropical wetlands have relied on medium-resolution or coarser satellite imagery, and required years of processing to complete (Giri et al., 2011). Further, detection of change in $10-30$ m pixels covering 100-900 m² each may be insufficient for identifying gain or loss before irreversible changes have already occurred (Klemas, 2013; Kuenzer et al., 2011). Addressing these challenges will require accurate, automated mapping of high-resolution images. With such imagery available, efforts must shift to address mapping efficiency while maintaining accurate products.

Accuracy assessments relied on GRPs collected during a field campaign as opposed to digitized points determined visually with independent remote sensing data. We prefer the former for its reliability, especially as the mixed nature of damaged mangrove makes it difficult

to accurately identify from pixels, although we acknowledge that digitized training and validation points would likely generate a larger body of GRPs. The accuracy assessment results of this case study reveal similarly accurate maps of healthy and degraded vegetation. The NN algorithm produced the most accurate overall map (85 %) versus 83 % for both DT and SVM. Individual class producer's accuracies, however, favored DT for healthy mangrove (91 % vs 88 % NN and 86 % SVM), NN for upland (75 % vs 69 % NN and 63 % DT), SVM for degraded vegetation (62 % vs 57 % NN and 38 % DT), DT for soil (97 % vs 92 % each NN and SVM), and all maps identified water to 100 % producer's accuracy. The relatively low-accuracy results for degraded vegetation likely reflect misclassification due to the inherently mixed spectral patterns of a highly altered and recovering habitat whereby adjacent areas are likely to exhibit variation in defoliation extent, surface substrate, and seedling germination. These results are similar to those of a previous study that compared NN and SVM methods with the classification and regression tree (CART) method to map urban area, deciduous forest, evergreen forest, agricultural land, and wetland (Shao and Lunetta, 2012). However, that work relied on existing land cover maps for training and validation. Such reference data presents an issue that must be addressed: Mapping novel target classes is not possible, and results will be skewed by any inaccuracies in the training map. Simply using historical land cover maps as a source of training data gives different results that depend on the input map used. McCarthy et al. (2015) demonstrated this issue using wetland maps developed separately by NOAA, the Southwest Florida Water Management District, and the National Wetland Inventory. The recommendation based on these results is that any underlying accuracies need to be disclosed and discussed when a particular training method is used for a specific classification approach.

While more accurate overall and in upland (NN) and degraded vegetation (SVM), machine learning approaches currently have a substantial drawback that must be considered before adopting for large-scale mapping: They require a suitably large training dataset to tune the algorithm (Scott et al., 2017). This requirement may be satisfied for a given study area if sufficient spectral libraries exist from which to draw training data. However, the library data would have to be calibrated consistently with the test dataset, contain matching or comparable spectral wavelength ranges, and represent the exact target classes. New approaches to address the issue of training data attempt to carryover existing training data from one region to another. Domain adversarial neural networks, for example, leverage transfer learning in an unsupervised setting to map areas that are independent and possibly quite distinct from the training collection area. While promising, applications thus far have only demonstrated sufficiency in broad characterization of image tiles that may not be applicable or transferrable to coastal habitat mapping (Huang et al., 2015).

Further, accurately isolating clouds and shadows (e.g. cast by buildings or tree canopies) is necessary when mapping very high-resolution imagery (Stratoulias et al., 2017). Doing so poses a challenge for machine-learning methods that may attempt to train such a classifier with inaccurate data due to the transient nature of clouds and

Table 2
Confusion Matrix for DT classifier results. Overall accuracy in bold (Kappa = 0.765).

		Reference Data						
		Soil	Degraded Mangrove	Upland	Healthy Mangrove	Water	Total	User's Accuracy
Classified Data	Soil	99	3	0	0	0	102	97 %
	Degraded Mangrove	1	8	2	2	0	13	62 %
	Upland	0	0	59	9	0	68	87%
	Healthy Mangrove	0	8	32	107	0	147	73%
	Water	2	2	0	0	23	27	85 %
	Total	102	21	93	118	23	357	
	Producer's Accuracy	97 %	38 %	63 %	91 %	100 %		**83 %**

Table 3
Confusion Matrix for SVM classifier results. Overall accuracy in bold (Kappa = 0.767).

		Reference Data						
		Soil	Degraded Mangrove	Upland	Healthy Mangrove	Water	Total	User's Accuracy
Classified Data	Soil	94	0	3	0	0	97	97 %
	Degraded Mangrove	2	13	2	5	0	22	59%
	Upland	3	1	64	11	0	79	81%
	Healthy Mangrove	0	7	24	102	0	133	77%
	Water	3	0	0	0	23	26	88 %
	Total	102	21	93	118	23	357	
	Producer's Accuracy	92 %	62 %	69 %	86 %	100 %		**83 %**

Table 4
Confusion Matrix for NN classifier results. Overall accuracy in bold (Kappa = 0.792).

		Reference Data						
		Soil	Degraded Mangrove	Upland	Healthy Mangrove	Water	Total	User's Accuracy
Classified Data	Soil	94	0	2	0	0	96	98%
	Degraded Mangrove	2	12	1	1	0	16	75 %
	Upland	4	3	70	13	0	90	78%
	Healthy Mangrove	0	6	20	104	0	130	80%
	Water	2	0	0	0	23	25	92 %
	Total	102	21	93	118	23	357	
	Producer's Accuracy	92 %	57 %	75 %	88 %	100 %		**85 %**

shadows. Decision-based methods that attempt to isolate a consistent pattern may also result in low accuracies where thin clouds and shadowed pixels retain a muted spectral signature of the underlying class. One method to account for this issue in isolated areas is to use a conservative index to assign a specific value that may be reassigned to the value of the predominant surrounding class during post-processing with a moving-window filter (McCarthy et al., 2018; Le Hégarat-Mascle and André, 2009). Future work for large-scale and time-series mapping will likely encounter cloud-cover issues, and will certainly encounter shadows, thereby necessitating that these classes be a focus of further algorithm development.

5. Conclusions

Modern versions of both traditional and machine-learning classification methods produce similarly accurate mapped products when distinguishing healthy from hurricane-degraded mangrove vegetation, but exhibit tradeoffs in development and application that must be considered for large-scale or time-series mapping progress. The DT method generally requires extensive front-end development, but may be iteratively refined and applied in a computationally efficient manner, especially so when leveraging the prodigious expansion of supercomputing technology. SVM and NN methods only require generation or acquisition of training data (i.e. digitized or field collected) that are ingested by an existing statistically robust algorithm to assign pixels to classes, but are limited by the spatio-temporal scope of such training data. Approaches are being developed to potentially train such a classifier using data collected independently from the area where the classifier will be applied, which could revolutionize the application of such methods.

As satellite and computational technologies advance, mapping at higher resolutions over larger scales and monitoring with time series will become much needed standard practice for conservation and resource management, among many other applications. Efforts to carryout accurate and efficient mapping must consider the tradeoffs and feasibility of available methods, and advance them with the considerations noted here.

Declaration of interests

The authors declare that they have no known competing financial interests or personal relationships that could have appeared to influence the work reported in this paper.

CRediT authorship contribution statement

Matthew J. McCarthy: Conceptualization, Methodology, Software, Validation, Formal analysis, Investigation, Resources, Data curation, Writing - original draft, Visualization, Funding acquisition. **Brita Jessen:** Conceptualization, Methodology, Software, Validation, Formal analysis, Investigation, Writing - review & editing, Funding acquisition. **Michael J. Barry:** Methodology, Validation, Resources, Writing - review & editing. **Marissa Figueroa:** Resources, Writing - review & editing. **Jessica McIntosh:** Methodology, Validation, Investigation, Resources, Writing - review & editing. **Tylar Murray:** Software, Investigation, Data curation, Writing - review & editing. **Jill Schmid:** Investigation, Writing - review & editing. **Frank E. Muller-Karger:** Resources, Writing - review & editing, Supervision, Project

administration, Funding acquisition.

Appendix A. Supplementary data

Supplementary material related to this article can be found, in the online version, at doi:https://doi.org/10.1016/j.jag.2020.102134.

References

Barbier, E.B., 2015. Valuing the storm protection service of estuarine and coastal ecosystems. Ecosyst. Serv. 11, 32–38. https://doi.org/10.1016/j.ecoser.2014.06.010.

Bergamaschi, P., Houweling, S., Segers, A., Krol, M., Frankenberg, C., Scheepmaker, R.A., Dlugokencky, E., Wofsy, S.C., Kort, E.A., Sweeney, C., et al., 2013. Atmospheric CH4 in the first decade of the 21st century: inverse modeling analysis using SCIAMACHY satellite retrievals and NOAA surface measurements. J. Geophys. Res. Atmos. 118, 7350–7369. https://doi.org/10.1002/jgrd.50480.

Bousquet, P., Ringeval, B., Pison, I., Dlugokencky, E.J., Brunke, E.G., Carouge, C., Chevallier, F., Fortems-Cheiney, A., Frankenberg, C., Hauglustaine, D.A., et al., 2011. Source attribution of the changes in atmospheric methane for 2006–2008. Atmos. Chem. Phys. 11, 3689–3700. https://doi.org/10.5194/acp-11-3689-2011.

Civco, D.L., 1993. Artificial neural networks for land-cover classification and mapping. Int. J. Geogr. Inf. Syst. 7, 173–186. https://doi.org/10.1080/02693799308901949.

Davidson, N.C., 2014. How much wetland has the world lost? Long-term and recent trends in global wetland area. Mar. Freshw. Res. 65. https://doi.org/10.1071/mf14173.

de Groot, R., Brander, L., van der Ploeg, S., Costanza, R., Bernard, F., Braat, L., Christie, M., Crossman, N., Ghermandi, A., Hein, L., et al., 2012. Global estimates of the value of ecosystems and their services in monetary units. Ecosyst. Serv. 1, 50–61. https://doi.org/10.1016/j.ecoser.2012.07.005.

Dlugokencky, E.J., Nisbet, E.G., Fisher, R., Lowry, D., 2011. Global atmospheric methane: budget, changes and dangers. Philos. Trans. A Math. Phys. Eng. Sci. 369, 2058–2072. https://doi.org/10.1098/rsta.2010.0341.

Friedl, M.A., McIver, D.K., Hodges, J.C.F., Zhang, X.Y., Muchoney, D., Strahler, A.H., Woodcock, C.E., Gopal, S., Schneider, A., Cooper, A., et al., 2002. Global land cover mapping from MODIS: algorithms and early results. Remote Sens. Environ. 83, 287–302.

Gedney, N., 2004. Climate feedback from wetland methane emissions. Geophys. Res. Lett. 31. https://doi.org/10.1029/2004gl020919.

Giri, C., Ochieng, E., Tieszen, L.L., Zhu, Z., Singh, A., Loveland, T., Masek, J., Duke, N., 2011. Status and distribution of mangrove forests of the world using earth observation satellite data. Glob. Ecol. Biogeogr. 20, 154–159. https://doi.org/10.1111/j.1466-8238.2010.00584.x.

Globe, D., 2010. Radiometric Use of WorldView-2 Imagery; Technical Note. Digital Globe, Westminster, CO, USA.

Hestir, E.L., Brando, V.E., Bresciani, M., Giardino, C., Matta, E., Villa, P., Dekker, A.G., 2015. Measuring freshwater aquatic ecosystems: the need for a hyperspectral global mapping satellite mission. Remote Sens. Environ. 167, 181–195. https://doi.org/10.1016/j.rse.2015.05.023.

Hird, J., DeLancey, E., McDermid, G., Kariyeva, J., 2017. Google earth engine, open-access satellite data, and machine learning in support of large-area probabilistic wetland mapping. Remote Sens. 9, 1315. https://doi.org/10.3390/rs9121315.

Huang, W., Hagen, S., Bacopoulos, P., Wang, D., 2015. Hydrodynamic modeling and analysis of sea-level rise impacts on salinity for oyster growth in Apalachicola Bay, Florida. Estuar. Coast. Shelf Sci. 156, 7–18. https://doi.org/10.1016/j.ecss.2014.11.008.s.

Klemas, V., 2013. Using remote sensing to select and monitor wetland restoration sites: an overview. J. Coast. Res. 289, 958–970. https://doi.org/10.2112/jcoastres-d-12-00170.1.

Kuenzer, C., Bluemel, A., Gebhardt, S., Quoc, T.V., Dech, S., 2011. Remote sensing of mangrove ecosystems: a review. Remote Sens. 3, 878–928. https://doi.org/10.3390/rs3050878.

Le Hégarat-Mascle, S., André, C., 2009. Use of Markov random fields for automatic cloud/shadow detection on high resolution optical images. ISPRS J. Photogramm. Remote Sens. 64, 351–366. https://doi.org/10.1016/j.isprsjprs.2008.12.007.

Liu, T., Abd-Elrahman, A., Morton, J., Wilhelm, V.L., 2018. Comparing fully convolutional networks, random forest, support vector machine, and patch-based deep convolutional neural networks for object-based wetland mapping using images from small unmanned aircraft system. GISci. Remote Sens. 55, 243–264. https://doi.org/10.1080/15481603.2018.1426091.

Lottering, R., Mutanga, O., Peerbhay, K., Ismail, R., 2019. Detecting and mapping Gonipterus scutellatus induced vegetation defoliation using WorldView-2 pan-sharpened image texture combinations and an artificial neural network. J. Appl. Remote Sens. 13. https://doi.org/10.1117/1.Jrs.13.014513.

McCarthy, M., Halls, J., 2014. Habitat mapping and change assessment of coastal environments: an examination of WorldView-2, QuickBird, and IKONOS satellite imagery and airborne LiDAR for mapping barrier island habitats. ISPRS Int. J. Geoinf. 3, 297–325. https://doi.org/10.3390/ijgi3010297.

McCarthy, M.J., Merton, E.J., Muller-Karger, F.E., 2015. Improved coastal wetland mapping using very-high 2-meter spatial resolution imagery. Int. J. Appl. Earth Obs. Geoinf. 40, 11–18. https://doi.org/10.1016/j.jag.2015.03.011.

McCarthy, M.J., Radabaugh, K.R., Moyer, R.P., Muller-Karger, F.E., 2018. Enabling efficient, large-scale high-spatial resolution wetland mapping using satellites. Remote Sens. Environ. 208, 189–201. https://doi.org/10.1016/j.rse.2018.02.021.

McLeod, E., Chmura, G.L., Bouillon, S., Salm, R., Björk, M., Duarte, C.M., Lovelock, C.E., Schlesinger, W.H., Silliman, B.R., 2011. A blueprint for blue carbon: toward an improved understanding of the role of vegetated coastal habitats in sequestering CO2. Front. Ecol. Environ. 9, 552–560. https://doi.org/10.1890/110004.

McNorton, J., Gloor, E., Wilson, C., Hayman, G.D., Gedney, N., Comyn-Platt, E., Marthews, T., Parker, R.J., Boesch, H., Chipperfield, M.P., 2016g. Role of regional wetland emissions in atmospheric methane variability. Geophys. Res. Lett. 43 (11), 433–444. https://doi.org/10.1002/2016gl070649.

Nisbet, E.G., Manning, M.R., Dlugokencky, E.J., Fisher, R.E., Lowry, D., Michel, S.E., Myhre, C.L., Platt, S.M., Allen, G., Bousquet, P., et al., 2019. Very strong atmospheric methane growth in the 4 years 2014–2017: implications for the Paris agreement. Global Biogeochem. Cycles 33, 318–342. https://doi.org/10.1029/2018gb006009.

Pison, I., Ringeval, B., Bousquet, P., Prigent, C., Papa, F., 2013. Stable atmospheric methane in the 2000s: key-role of emissions from natural wetlands. Atmos. Chem. Phys. 13, 11609–11623. https://doi.org/10.5194/acp-13-11609-2013.

Purkis, S.J., Gleason, A.C.R., Purkis, C.R., Dempsey, A.C., Renaud, P.G., Faisal, M., Saul, S., Kerr, J.M., 2019. High-resolution habitat and bathymetry maps for 65,000 sq. km of Earth's remotest coral reefs. Coral Reefs 38, 467–488. https://doi.org/10.1007/s00338-019-01802-y.

Radabaugh, K.R., Moyer, R.P., Chappel, A.R., Dontis, E.E., Russo, C.E., Joyse, K.M., Bownik, M.W., Goeckner, A.H., Khan, N.S., 2019. Mangrove damage, delayed mortality, and early recovery following hurricane irma at two landfall sites in Southwest Florida, USA. Estuaries Coasts. https://doi.org/10.1007/s12237-019-00564-8.

Scott, G.J., England, M.R., Starms, W.A., Marcum, R.A., Davis, C.H., 2017. Training deep convolutional neural networks for land–cover classification of high-resolution imagery. IEEE Geosci. Remote. Sens. Lett. 14, 549–553. https://doi.org/10.1109/lgrs.2017.2657778.

Shao, Y., Lunetta, R.S., 2012. Comparison of support vector machine, neural network, and CART algorithms for the land-cover classification using limited training data points. ISPRS J. Photogramm. Remote Sens. 70, 78–87. https://doi.org/10.1016/j.isprsjprs.2012.04.001.

Stratoulias, D., Tolpekin, V., de By, R., Zurita-Milla, R., Retsios, V., Bijker, W., Hasan, M., Vermote, E., 2017. A workflow for automated satellite image processing: from raw VHSR data to object-based spectral information for smallholder agriculture. Remote Sens. 9. https://doi.org/10.3390/rs9101048.

Turner, A.J., Jacob, D.J., Benmergui, J., Wofsy, S.C., Maasakkers, J.D., Butz, A., Hasekamp, O., Biraud, S.C., 2016. A large increase in U.S. methane emissions over the past decade inferred from satellite data and surface observations. Geophys. Res. Lett. 43, 2218–2224. https://doi.org/10.1002/2016gl067987.

Turpie, K.R., 2013. Explaining the spectral red-edge features of inundated marsh vegetation. J. Coast. Res. 290, 1111–1117. https://doi.org/10.2112/jcoastres-d-12-00209.1.

Walcker, R., Laplanche, C., Herteman, M., Lambs, L., Fromard, F., 2019. Damages caused by hurricane Irma in the human-degraded mangroves of Saint Martin (Caribbean). Sci. Rep. 9, 18971. https://doi.org/10.1038/s41598-019-55393-3.

Whyte, A., Ferentinos, K.P., Petropoulos, G.P., 2018. A new synergistic approach for monitoring wetlands using Sentinels -1 and 2 data with object-based machine learning algorithms. Environ. Model. Softw. 104, 40–54. https://doi.org/10.1016/j.envsoft.2018.01.023.